

COMPARISON OF DIFFERENT SPATIAL/ANGULAR AGGLOMERATION MULTIGRID SCHEMES FOR RADIATIVE HEAT TRANSFER COMPUTATIONS

Georgios N. Lygidakis¹ and Ioannis K. Nikolos²

^{1,2} Technical University of Crete, School of Production Engineering and Management
University Campus, Chania, GR-73100, Greece

¹e-mail: glygidakis@isc.tuc.gr

²e-mail: jnikolo@dpem.tuc.gr

Keywords: Radiative Heat Transfer, Finite-Volume Method, Multigrid Scheme, Spatial/Angular Agglomeration, FAS, FMG.

Abstract. *During the past decade the 3D unstructured grids have become an important tool for radiative heat transfer simulations, extending their applications to even more complex enclosures. Nevertheless, the corresponding solvers appear to be inferior in terms of efficiency, compared to those for structured meshes. One remedy to this shortcoming appears to be the agglomeration multigrid method, based on the solution of the numerical problem on successively coarser spatial and angular resolutions, derived from the initial finest ones through the fusion of their neighbouring control volumes and control angles respectively. Considering this state, the enhancement of an in-house academic solver with different spatial/angular agglomeration multigrid schemes to accelerate the finite-volume method for the prediction of radiative heat transfer, is reported in this study. The incorporated multigrid methods are based on the relaxation of radiative transfer equation with the FAS approach, considering though different types of sequentially coarser spatial and angular resolutions, as well as different V-cycle types. More specifically, a nested, a uniform and an alternate scheme were developed, while they were examined in conjunction with the $V(1,0)$, $V(1,1)$, $V(2,0)$ and $V(2,1)$ V-cycles types. To further accelerate the numerical solution, a combined FMG-FAS strategy was included, according to which the whole procedure begins from the coarsest discretization (spatial and angular) and as the number of iterations is increased the FAS extends to the finer resolutions, up to the initial finest one. The proposed numerical schemes were validated against a benchmark test case, considering radiative heat transfer through a strongly scattering medium in a cubic enclosure with highly reflecting surfaces. The obtained results reveal the superiority of the nested scheme along with the $V(2,0)$ -cycle type strategy, while they highlight the significant contribution of the angular extension of the multigrid technique.*

1 INTRODUCTION

During the last decade the three-dimensional unstructured grids have become an important tool for radiative heat transfer computations, extending their applications to more complex geometries, like combustion chambers. Although unstructured meshes offer the largest possible flexibility in the treatment of complicated enclosures, along with the minimum user interaction for their generation/adaptation, the corresponding solvers appear to be inferior in terms of efficiency, compared to those for structured grids [1]. One remedy to this shortcoming is the multigrid method, originally developed by Brandt [2] to increase the convergence rate of the numerical solution of elliptic problems, e.g. of incompressible fluid flow problems in CFD (Computational Fluid Dynamics). Since then it has been applied though to various types of computational simulations, e.g., compressible fluid flow [3-5], radiative heat transfer [6-8], etc. Its main concept depends on the construction of coarser resolutions, in order the low-frequency errors at the finest discretization to become high-frequency ones at the coarser ones, and as such to be damped in a more efficient way [1, 3, 6]. Besides multigrid method's significant contribution in test cases with unstructured grids, it was additionally revealed to be a valuable tool for simulations involving higher-order accurate spatial schemes [6, 7, 9-11] or higher-order governing equations [12]. Various types of the multigrid methodology have been developed during the past years, whose differences are identified mainly on the way the coarser discretizations are generated, as well as on the relation associating the successive grid resolutions [1, 6].

The agglomeration multigrid method, originally proposed by Lallemand [13], appears to be one of the most widely implemented schemes. It considers a sequence of coarser spatial resolutions with polyhedral elements, derived through the fusion of neighboring control volumes of their finer levels in an arbitrary way (isotropic agglomeration) [6]. Nevertheless, the aforementioned agglomeration strategy has been identified to lead to reduced performance in test cases involving hybrid grids with highly stretched elements on boundary surfaces [14]. A semi-coarsening or directional coarsening agglomeration method was proposed by Mavriplis [14] to mitigate this drawback. According to this technique the nodes of prismatic and hexahedral elements are treated separately, i.e., their control cells are merged only if they are aligned with the normal to the boundary direction [1]; for the rest nodes the aforementioned isotropic strategy is applied. As a result, the grid anisotropy, caused by the utilization of prismatic or hexahedral elements, is moderated [15]. Another popular approach is the full-coarsening directional agglomeration [1, 4, 16, 17], according to which the boundary control cells are fused initially, while a line-agglomeration step is then performed, for merging the prismatic or hexahedral control volumes along implicit lines, directly above the corresponding already agglomerated boundary ones. As a result, a deeper reduction of DoFs (Degrees of Freedom) is succeeded and consequently further acceleration is gained, without though the produced discretizations to differentiate significantly from the initial topology. Specifically for radiative heat transfer simulations, which consider the solution of RTE (Radiative Transfer Equation), for each control cell and each control angle, an angular extension of the aforementioned agglomeration strategy has been proposed by the authors, either coupled with the spatial one or not [6, 7]. According to this methodology, angularly coarser resolutions are also generated (besides the spatially coarser ones), resulting in further improvement of the computational performance of the iterative methodology, via a nested spatial/angular agglomeration multigrid scheme [6, 7].

As far as the relation associating each two successive resolutions is concerned the FAS (Full Approximation Scheme) approach is revealed to be the most widely applied one [1, 3]. It considers the relaxation of the governing PDEs (Partial Differential Equations) only at the ini-

tial finest level, while at the coarser ones an approximate version of the same PDEs is solved [3], accomplishing gradually a V- or W-cycle scheme. The computed variables and flux balances are restricted (in terms of smoothing) from the finer to the coarser mesh, while the corresponding calculated corrections are prolonged (in terms of interpolation) from the coarser to the finer one [1, 3, 4, 6]. In case of multigrid accelerated radiative heat transfer problems, considering additionally angularly coarser resolutions, the approximation of the angularly coarser PDEs is performed by employing the FAS scheme much in the same way to the spatial ones [6, 7]. In order to gain additional acceleration, a combined FMG-FAS (Full Multigrid-Full Approximation Scheme) approach can be implemented [1, 4, 15]. According to this method the FAS V-cycle is incorporated in the FMG process; the whole procedure begins from the coarsest grid and, as the number of iterations is increased, the finer FAS levels are added up to the initial finest one [1, 4, 15].

In this work the development and comparison of different spatial/angular agglomeration multigrid schemes for the acceleration of FVM radiative heat transfer computations, is reported. It is based upon a previous work of the authors [6, 7], incorporating though further enhancements, namely different sequences of spatial and angular coarser resolutions, different V-cycle types, a full-coarsening directional agglomeration strategy and a combined FMG-FAS approach. More precisely, the nested, uniform, and alternate schemes are compared. According to the first nested one (reported in [6, 7]) the angular V-cycle is accomplished at each step of the spatial one. If the uniform scheme is selected each coarser resolution is constructed by simultaneously coarsening its finer one spatially and angularly, while in case of the alternate technique each coarser level is obtained from the finer one by coarsening it either in spatial or angular dimension. As far as the different V-cycle types are concerned the V(1,0), V(1,1), V(2,0) and V(2,1) are assessed; the first number in parentheses denotes the number of relaxations performed prior to restriction, while the second one denotes the corresponding number of relaxations after the prolongation [6]. For simulations involving hybrid grids, in order increased accuracy to be achieved in regions with prismatic elements [18], a full-coarsening directional agglomeration strategy is additionally developed [1, 4, 5]. It succeeds greater reduction of DoFs and consequently greater acceleration, comparing to this obtained with isotropic agglomeration methodology. Finally, a combined FMG-FAS approach is developed and tested against the only-FAS technique [1, 4, 15]; it considers the division of the whole procedure in two stages, the preliminary and the main one [1, 4, 15]. It begins from the coarsest resolution (preliminary stage) while, as the number of iterations is increased, the finer FAS levels are added up to the initial finest one (main stage) [1, 4, 15]. The proposed numerical schemes are evaluated against a benchmark test case, considering radiative heat transfer through a strongly scattering medium in a cubic enclosure with highly reflecting surfaces [19]. According to the produced results the nested spatial/angular scheme along with the V(2,0)-cycle type appears to be the preferred choice for such simulations. Furthermore, they highlight the significant contribution of the angular extension of the multigrid technique.

2 RADIATIVE HEAT TRANSFER COMPUTATION

The radiative intensity I_p of a node p at position r and time t along a path s through an absorbing, emitting and scattering gray medium is obtained by the time-dependent RTE as follows [10, 11, 20, 21]

$$\frac{1}{c} \frac{dI_p(\vec{r}, \hat{s})}{dt} + \frac{dI_p(\vec{r}, \hat{s})}{ds} = -(k_\alpha + \sigma_s) I_p(\vec{r}, \hat{s}) + k_\alpha I_b(\vec{r}) + \frac{\sigma_s}{4\pi} \int_{4\pi} I_p'(\vec{r}, \hat{s}_i') \Phi(\hat{s}, \hat{s}_i') d\omega \quad (1)$$

where c is the propagation speed of radiation, while k_α and σ_s are the absorption and scattering coefficient respectively [10, 11]. The LHS terms express the radiative intensity change rate per ray direction and time, while the RHS expresses its attenuation by absorption and scattering processes (first term), and its augmentation by blackbody energy (second term) and scattering phenomenon (third term) [6, 10]. Despite the presence of the temporal term, the aforementioned expression can be employed for both steady-state and transient problems [6, 10, 11, 20].

The finite-volume method is applied for the discretization of the computational field and consequently for the solution of the RTE [6, 12]; therefore, the computational domain has to be discretized both spatially and angularly. A node-centered median dual control volume method is employed for the spatial discretization, according to which the construction of the control cell of a node is achieved by connecting the lines defined by the edge midpoints, the barycenters of faces and the barycenters of elements sharing this node [3, 18]. Angular discretization is succeeded by dividing the directional domain, represented by a *sphere* in three dimensions, into a discrete number of solid control angles with lines of constant longitude and latitude [18, 21]; an equal division strategy is followed in this work, hence, the 4π steradians derive $N_\theta \times N_\phi$ control angles [6, 10, 18]. Thus, equation (1) is integrated over the control volume of each node p and each solid control angle $\Delta\Omega^{mn}$ deriving the following formulation [10]

$$\Delta I_p^{mn} \frac{V_p \Delta\Omega^{mn}}{c\Delta t} + \sum_i I_i^{mn} D_{ci}^{mn} \Delta A_i = \left[-(k_\alpha + \sigma_s) I_p^{mn} + S_R^{mn} \right] V_p \Delta\Omega^{mn} \quad (2)$$

where V_p is the volume of the examined control cell. The source term S_R^{mn} , which includes the contribution of the blackbody energy and the scattering phenomenon from other solid control angles, is expressed as [10]

$$S_R^{mn} = k_\alpha I_b + \frac{\sigma_s}{4\pi} \int_{4\pi} I_p^{m'n'} \Phi(m'n', mn) d\omega \quad (3)$$

where Φ denotes the Scattering Phase Function. If isotropic scattering is assumed, a constant value is assigned to it [18, 22]; alternatively, medium's anisotropic attitude has to be modelled, e.g. using Legendre polynomials (as in this study) [18, 22]. Finally, D_{ci}^{mn} is the directional weight, defined by the examined control angle $\Delta\Omega^{mn}$ and the unit normal vector of the examined control volume surface, while I_i^{mn} is the corresponding radiative intensity [10, 11]. For its definition the step scheme is adopted in this work, according to which the radiative intensity at a downstream face is set equal to that of the upstream node; this is expressed for two neighboring nodes p and q as [6, 10]

$$I_i^{mn} D_{ci}^{mn} = I_p^{mn} D_{ci,out}^{mn} + I_q^{mn} D_{ci,in}^{mn} \quad (4)$$

where $D_{ci,out}^{mn}$ denotes the directional weight going outwards the examined control volume (of node p), while $D_{ci,in}^{mn}$ the corresponding weight coming into the same cell [6]. Considering this scheme, an edge-based data structure is used to reduce the computational load [3]. Furthermore, in order to alleviate the overhang problem, derived by the combination of unstructured grids with the angular division of the computational domain, the pixelation method is applied transforming appropriately the aforementioned weights [10, 11]. In that way the effect of overlapped directional weights is considerably reduced and the accuracy of the final solution is increased.

For the same accuracy reasons, a higher-order accurate spatial scheme is implemented reducing the effect of false scattering, derived by the spatial discretization of the computational field. Particularly, a second-order scheme is used in this work, based on the well-established

in CFD MUSCL (Monotone Upstream Scheme for Conservation Laws) methodology [23]. Therefore, the values of radiative intensity at the RHS of equation (4) are reconstructed prior to the implementation of the step scheme; the required gradients are obtained with the Green-Gauss linear representation method [10]. Moreover, in order to control the aforementioned reconstructed values, especially at boundary areas entailing high intensity gradients, the scheme is coupled with the Van Albada-Van Leer [23] or the Min-mod [24] slope limiters [10, 11].

Finally, the appropriate contributions of the boundary conditions are added to the fluxes of the corresponding nodes; they are computed in an implicit way applying the step scheme between the examined node and a *ghost* node outside the computational field [10, 11]. Opaque and diffusive boundary surfaces, as well as mirroring ones are assumed in this study [10, 11].

Since the required flux balance has been obtained for each node and each solid control angle, equation (2) is transformed as [10, 11]

$$\Delta I_p^{mn} \frac{V_p \Delta \Omega^{mn}}{c \Delta t} = R_p^{mn} \quad (5)$$

where R_p^{mn} is the fluxes sum, while Δt is the pseudo-time step defined via a local time-stepping technique [3, 10, 11]. For the iterative relaxation of equation (5) an explicit second-order temporal accurate scheme, using a four-stage Runge-Kutta method (RK(4)) [25], is employed. Besides the local time-stepping technique and the edge-based data structures, further acceleration of the solution process is obtained with parallel processing, based on the domain decomposition approach and the MPI (Message Passing Interface) library functions [18, 26, 27].

3 THE SPATIAL/ANGULAR AGGLOMERATION MULTIGRID SCHEME

3.1 Spatial/angular agglomeration strategy

The first issue to be defined for the multigrid accelerated solution of RTE is the agglomeration strategy, i.e., the methodology which has to be applied for the generation of the sequence of the coarser resolutions. Similar procedures are followed for the construction of both the coarser spatial and angular discretizations. They are performed on a topology-preserving framework at each partition, in which the initial grid is divided for parallel processing [1, 6]; they are confined though by predefined limitations, ensuring consistency of the restriction and prolongation processes [1, 6].

Concerning the spatial agglomeration strategy, a similar to the advancing front technique is implemented, as the whole procedure begins from the solid wall boundary nodes, while it extends gradually to the internal ones [1, 6]; the starting point is justified by the fact that the proposed spatial algorithm was initially developed for CFD simulations [1, 4]. If no such boundary nodes are present to the examined sub-grid, the process begins from the *core* nodes at the overlapping regions (among the examined partition and its adjacent ones) [10, 11, 18]. As mentioned above, predefined rules limit though this procedure, e.g., a boundary node can be merged only with another boundary node of the same surface type, an internal node can be fused only with its neighboring also internal nodes, etc. [1, 6]. Taking into account those limitations the isotropic agglomeration procedure begins with the construction of the so-called *seed* list, including the solid wall boundary nodes. A loop is performed over them, examining their eligibility for fusion with their adjacent non-agglomerated yet ones; if no constraint is identified they are merged with their neighboring ones creating *supernodes*, while if a limitation exists they are simply transferred to the next multigrid level as *singleton supernodes* [1,

6]. A new list is then constructed including the nodes touched by the agglomeration front, which are actually the adjacent ones to the already examined and agglomerated nodes, while at next the previous step of examination and fusion is repeated. The procedure is assumed accomplished when all the *core* nodes have been examined. The *ghost* nodes are not included to the main agglomeration process, but they are fused according to the merging path of their corresponding *core* nodes at the adjacent partitions; as a result, virtual *ghost supernodes* are produced [1, 6]. The procedure continues with the construction of the corresponding *superedges*, connecting the derived *supernodes* and representing the interfaces of their control cells. In case an even coarser grid is required, the whole process is repeated. Further details for the applied isotropic spatial agglomeration procedure can be found in [1] and [6].

As mentioned in Introduction, the isotropic agglomeration strategy appears to be less effective in test cases involving hybrid grids, with highly stretched elements (prisms or hexahedra) at boundary surfaces [1, 4, 5, 14-17]; the latter are employed in order increased accuracy to be obtained at those areas [18]. Thus, a full-coarsening directional agglomeration procedure was also incorporated to the proposed algorithm, which is based on the methodology of Nishikawa and Diskin [5]. Further modifications have been included though; the agglomeration process isn't limited across the sub-domains' internal boundaries, allowing virtual *ghost supernodes* to be generated, while an additional limitation prohibits the fusion process of the control cells at prismatic layers in order the topology of the initial grid to be preserved more accurately [1]. Similarly to isotropic agglomeration, the directional one begins with the construction of the initial *seed* list, containing though the boundary nodes of only the prismatic elements [1, 5]. Since they are examined and merged in *supernodes*, a new list is created, filled with the nodes of the next prismatic layer; the latter are fused according to the agglomeration path of their corresponding boundary nodes, constructing the so-called implicit lines [1, 5]. The previous steps are repeated until all the prismatic nodes have been examined for fusion; the isotropic method is applied then for the rest nodes (tetrahedral and pyramidal) [1].

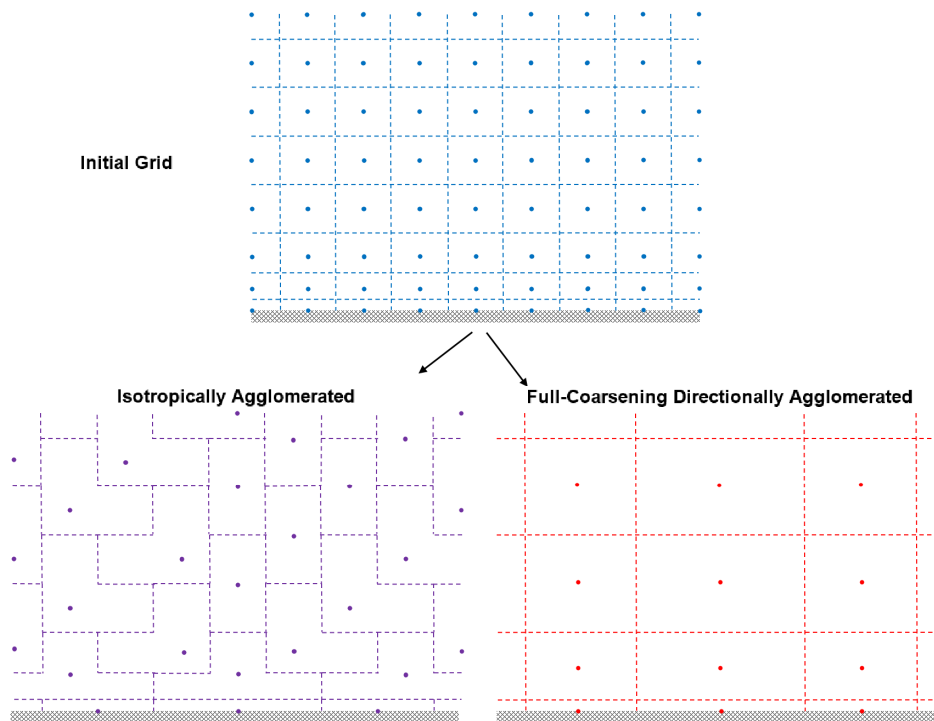


Figure 1: Isotropic and full-coarsening directional agglomeration of a 2D quadrilateral grid.

Figure 1 illustrates a schematic example of the previously described directional procedure (right), compared with this of the corresponding isotropic one (left). It is obvious that directional agglomeration preserves more accurately the topology of the initial grid; on the other hand, the isotropic approach derived a mesh with a topology modified compared to the initial one, due to the arbitrary polyhedral control cells it entailed. Further details for the aforementioned full-coarsening directional agglomeration procedure can be found in [1].

As far as the angular agglomeration is concerned, a similar to the spatial strategy is followed [6]. For the construction of each coarser resolution, every two successive control angles in both azimuthal and polar directions are fused, deriving new solid control *superangles*. Considering the equal separation strategy, followed for the division of the initial directional domain, each coarser level includes the one quarter of the number of solid control angles of its finer one [6]. The procedure is limited though by only one predefined constraint (unlike the spatial process), defining that only the control angles belonging to the same quadrant of the directional *sphere* can be fused together [6]. In that way consistency during the restriction and prolongation processes is ensured [6]. A more detailed description of the angular agglomeration strategy can be found in [6].

3.2 The spatial/angular agglomeration multigrid FAS approach

As mentioned in Introduction, this study aims to compare different combined spatial/angular agglomeration multigrid schemes for the acceleration of FVM radiative heat transfer computations. Particularly, three such schemes have been developed, namely a uniform, an alternate and a nested scheme. Their differences focus on the sequence of the spatial and angular levels, employed during the V-cycle of the FAS method. The procedures of the generation of the successively coarser resolutions (spatial and angular) as well as of the solution strategy (implementation of the second-order spatial accurate scheme and fix-up method, evaluation of directional weights and pixelation coefficients, etc.) are performed in the same way for all the developed schemes [6].

As far as the uniform spatial/angular agglomeration multigrid scheme is concerned, each coarser resolution is constructed by simultaneously coarsening its finer one spatially and angularly. According to the FAS approach, the solution procedure begins with the relaxation of equation (5) with the Runge-Kutta method at the initial finest resolution, while at next the values of the nodal fluxes and radiative intensity are restricted to the next coarser level as follows [6]:

$$\begin{aligned} R_{P,restricted}^{MN} &= (I_R)_{h,mn}^{H,MN} R_p^{mn} = \sum R_p^{mn} \\ I_{P,restricted}^{MN} &= (I_I)_{h,mn}^{H,MN} I_p^{mn} = \frac{\sum I_p^{mn} \cdot V_p \cdot \Delta\Omega^{mn}}{V_p \cdot \Delta\Omega^{MN}} \end{aligned} \quad (6)$$

Actually, a simple summation operator is applied for flux balances, considering both the included control cells and solid control angles. The corresponding operator for the values of radiative intensity defines a spatial-angular averaging process instead. Since the restriction process is accomplished, a similar to equation (5) relation is relaxed for this level (H, MN); its RHS is substituted though by the following value

$$R_{P,FAS}^{MN} = R_p^{MN} (I_p^{MN}) + \underbrace{\left[R_{P,restricted}^{MN} - R_p^{MN} (I_{P,restricted}^{MN}) \right]}_{A_H^{MN}} \quad (7)$$

where the first term denotes the fluxes of the agglomerated *supernode* P computed at this level (H, MN) similarly to the initial finest one using the previously constructed *superedges* [1, 6]. The forcing function A_H^{MN} includes the restricted fluxes to the *supernode* P and the fluxes of the same node, computed with the restricted values of radiative intensity from the finer resolution. It is quite obvious that for the first internal iteration of the Runge-Kutta scheme, the RHS term equals the restricted from the finer level flux balance, confirming in that way the approximation character of the FAS approach [1, 3, 6]. The aforementioned procedure of relaxation and restriction are repeated up to the coarsest generated resolution, while at next the obtained corrections are prolonged to the next finer level applying a simple point-injection scheme as [1, 3, 6]

$$(I_p^{mn})^{l+} = (I_p^{mn})^l + \Delta I_p^{mn} = (I_p^{mn})^l + (I_l)_{H, MN}^{h, mn} \Delta I_P^{MN} = (I_p^{mn})^l + (I_P^{MN} - I_{P, restricted}^{MN}) \quad (8)$$

The prolongation procedure is repeated similarly up to initial finest level, at which point the FAS V-cycle gets accomplished [1]. Figure 2 depicts a schematic representation of the aforementioned uniform method with a V(1,0)-cycle type and two spatial-angular coarser levels.

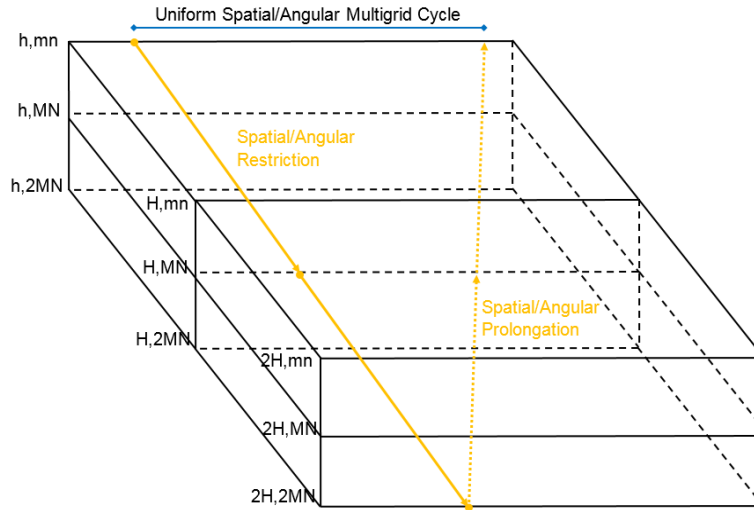


Figure 2: Uniform spatial/angular agglomeration multigrid cycle.

It should be highlighted that an equal number of coarser spatial and angular discretizations has to be used for the implementation of this approach. However, in most test cases, more spatial resolutions than angular ones can be generated [7]; to alleviate this shortcoming the coarsest generated angular discretization can be employed for the next coarser spatial levels too.

The alternate spatial/angular agglomeration multigrid scheme defines instead an alternation of spatial and angular coarsening at the sequence of FAS levels; as mentioned in Introduction, each coarser level is obtained from the finer one by coarsening it either in spatial or angular dimension. The whole procedure begins again with the solution of equation (5) at the initial finest level (spatially and angularly), while at next the nodal fluxes and radiative intensities are restricted to the next spatially coarser grid; no angular coarsening has been performed to this level. Since the solution is obtained at this discretization, the derived fluxes and radiative intensities are restricted to the next coarser level, provided with angular coarsening only. The aforementioned steps are repeated alternatively up to the coarsest resolution (spatially and angularly), while at next the corrections are prolonged accordingly, i.e., alternatively, up to the

initial spatially and angularly finest level. The operators, used for the aforementioned processes, are the same applied for the only-spatial or the only-angular agglomeration multigrid schemes [6]. Similarly to the uniform approach an equal number of coarser spatial and angular discretizations has to be used for the implementation of this scheme. Figure 3 includes a schematic representation of the previously described alternate method with a V(1,0)-cycle type and two spatial/angular coarser levels.

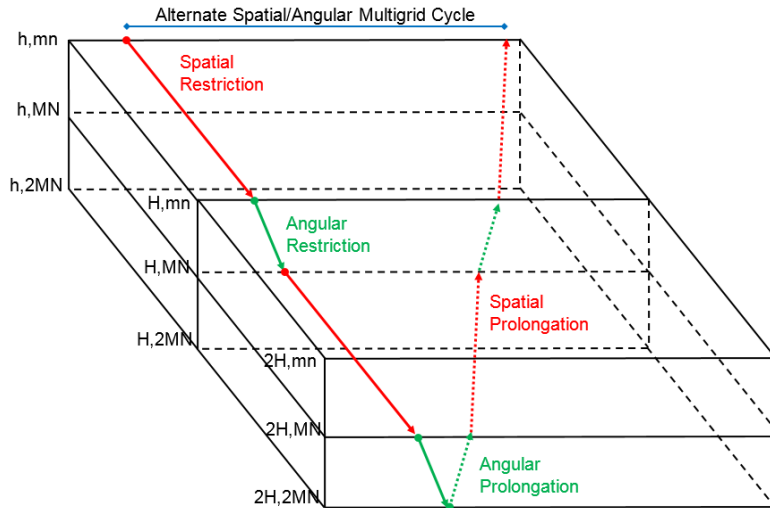


Figure 3: Alternate spatial/angular agglomeration multigrid cycle.

Besides the aforementioned schemes, a nested spatial/angular agglomeration multigrid scheme is assessed in this study, originally proposed in [6]. According to this approach, a complete angular FAS V-cycle is executed in each level of the spatial FAS V-cycle; the spatial and angular, restriction and prolongation, operators are applied similarly to the only-spatial and only-angular multigrid schemes [6]. Figure 4 illustrates its schematic representation, considering a V(1,0)-cycle type and two spatial/angular coarser levels. More details for the implementation of the nested spatial/angular agglomeration multigrid method can be found in [6].

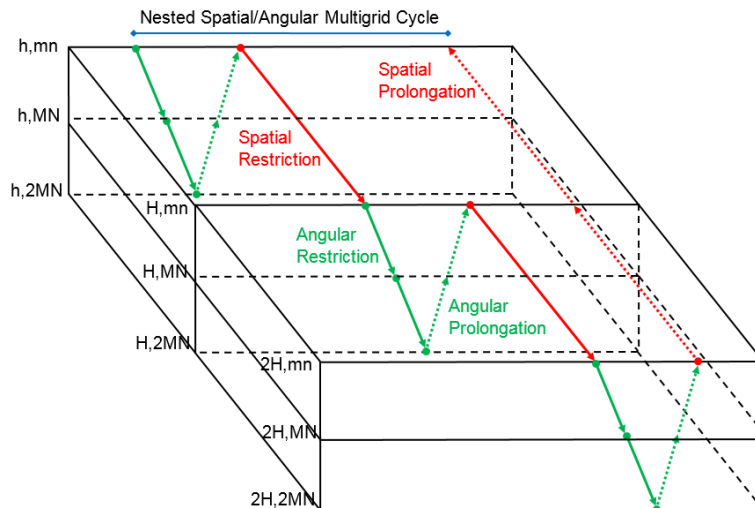


Figure 4: Nested spatial/angular agglomeration multigrid cycle.

3.3 FAS V-cycle types

Different V-cycle types are assessed in this study as well, namely the V(1,0), V(1,1), V(2,0) and V(2,1). The first number in parentheses denotes the number of relaxations performed prior to restriction, while the second denotes the corresponding number after the prolongation [1, 3]. Depending mainly on the implemented iterative procedure, as well as on the encountered problem's nature, various V-cycle types have been reported in the open literature as the most appropriate for them [1, 3, 5, 14-17]. For example, if an explicit iterative scheme is applied for an inviscid compressible fluid flow simulation a V(1,0)-cycle is usually preferred, while in case of a turbulent flow problem along with an implicit method, a V(2,1) appears to be the commonly preferred choice [1, 3]. As such, the four aforementioned V-cycle types have been incorporated in the proposed solver to study their effect on the code's computational efficiency.

3.4 The combined FMG-FAS agglomeration multigrid approach

A combined FMG-FAS agglomeration multigrid approach was also developed to further accelerate the solution procedure of the radiative heat transfer problems [1, 3, 4, 15]. Independently of the employed FAS scheme (only-spatial, only-angular, uniform, alternate or nested), it considers the division of the whole procedure in two stages, the preliminary and the main one [1, 4, 15]. As such, the solution process begins from the coarsest resolution and as the number of iterations/cycles is increased the FAS is extended to the next finer level, using the derived solution by the coarsest discretization as an initial guess [1]. In that way a cheaper initial condition is obtained, compared to the usually used uniform one [3]; for the interpolation of the solution the same single point-injection scheme, used for the prolongation process, is applied. The FAS solution process is continued, including only the two coarsest resolutions, while as the number of iterations/cycles is increased again, the previous steps are repeated adding successively more FAS levels up to the initial finest discretization, at which point the preliminary stage ends and the main one begins [1]. For simplicity reasons, in combined spatial/angular agglomeration multigrid schemes, the spatial and angular resolutions are extended simultaneously to their finer ones during the preliminary stage (similarly to the procedure followed for the uniform approach). Finally, the number of multigrid cycles/iterations performed during the preliminary stage may differ depending on the implemented multigrid scheme (only-spatial, only-angular, uniform, alternate or nested).

4 VALIDATION RESULTS

For the evaluation of the efficiency improvement, contributed by the different combinations of the proposed multigrid schemes (i.e., by employing the uniform, alternate, or nested scheme, different V-cycle types, and the combined FMG-FAS method), a benchmark test case was encountered, considering radiative heat transfer in a cubic enclosure with edge length equal to unity [7, 10, 19]. A schematic representation of the cubic geometry is depicted in Figure 5. The included cold medium is assumed purely scattering ($\sigma_s=1m^{-1}$, $k_a=0m^{-1}$, $T_m=0K$). The wall surfaces are considered similarly cold ($T_w=0K$), except for the bottom face at which a constant heating energy is implemented ($E=1W/m^2$), while for the bases normal to the y-direction mirroring boundary conditions are imposed [7, 10, 19]. The computational domain is represented by a hybrid grid, composed of 22,500 nodes, 65,480 tetrahedra and 19,460 prisms; for angular discretization the directional domain is divided in 16 azimuthal and 8 polar angles. Parallel processing was performed on a workstation with an AMD FX^(tm)-8350 eight-core processor at 4.00 GHz, while the initial mesh was divided in two sub-domains. In order to alleviate the overhang problem the pixelation method was implemented, while false

scattering effect was reduced with the incorporated second-order spatial accurate scheme, coupled with the Min-mod limiter [10, 11].

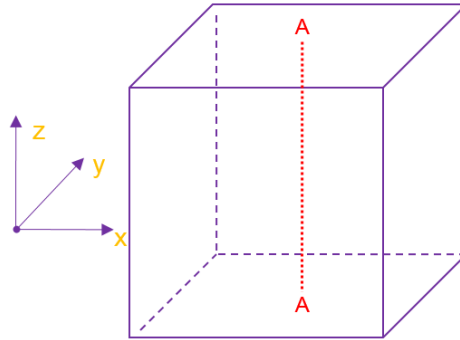


Figure 5: Geometry of the cubic enclosure.

Prior of validating the efficiency improvement, the accuracy of the proposed solver was assessed. The medium is assumed to exhibit anisotropic scattering behavior, which is modelled with the F2 scattering phase function, based on the Legendre polynomials [18, 19]. Two simulations were encountered for the evaluation of solver’s accuracy, in which different values of wall emissivity ϵ_w were assumed, namely 1.0 and 0.1 . In Figure 6 the extracted distributions of dimensionless incident radiative heat flux along the A-A line are illustrated, compared to the corresponding ones reported by Kim and Lee [19]. It is obvious that a very good agreement has been achieved. The second test case (with wall emissivity equal to 0.1) required much more computation time, compared to the first one, due to the increased radiation exchange between the discretized solid control angles [7]. Therefore, it was selected in order the efficiency evaluation simulations to be conducted with.

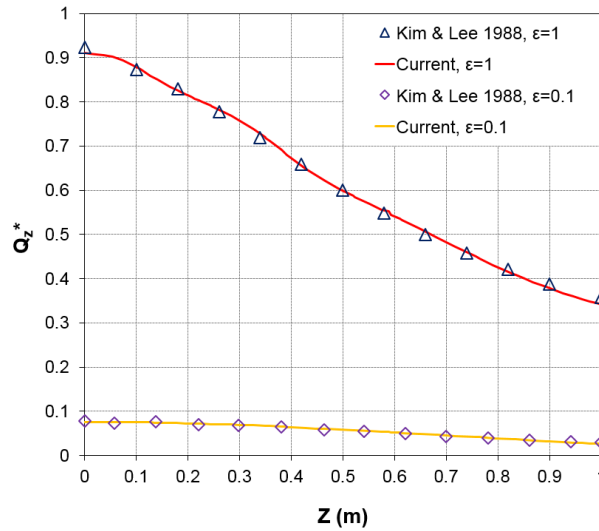


Figure 6: Distribution of the dimensionless incident radiative heat flux along the line A-A for two different values of wall emissivity ($\epsilon_w=1.0$ and $\epsilon_w=0.1$).

For the validation of the computational performance’s improvement the radiative intensity residual has to be computed at each multigrid cycle k [7]

$$residual = \frac{\sum_{p=1}^{N_p} \sum_{m=1}^{N_\theta} \sum_{n=1}^{N_\varphi} |I_p^{mn,k+1} - I_p^{mn,k}|}{N_p N_\theta N_\varphi} \quad (9)$$

where N_p denotes the number of nodes, while N_θ and N_φ the number of polar and azimuthal control angles, respectively, all of them regarding the initial finest resolution (spatially and angularly). Besides the contribution of the combined spatial/angular agglomeration multigrid schemes, developed in this study, this of the only-spatial and only-angular approaches was validated too. The notation SxAy, originally proposed in [7], is used in this work as well, where x denotes the number of spatial multigrid levels, while y the number of angular ones.

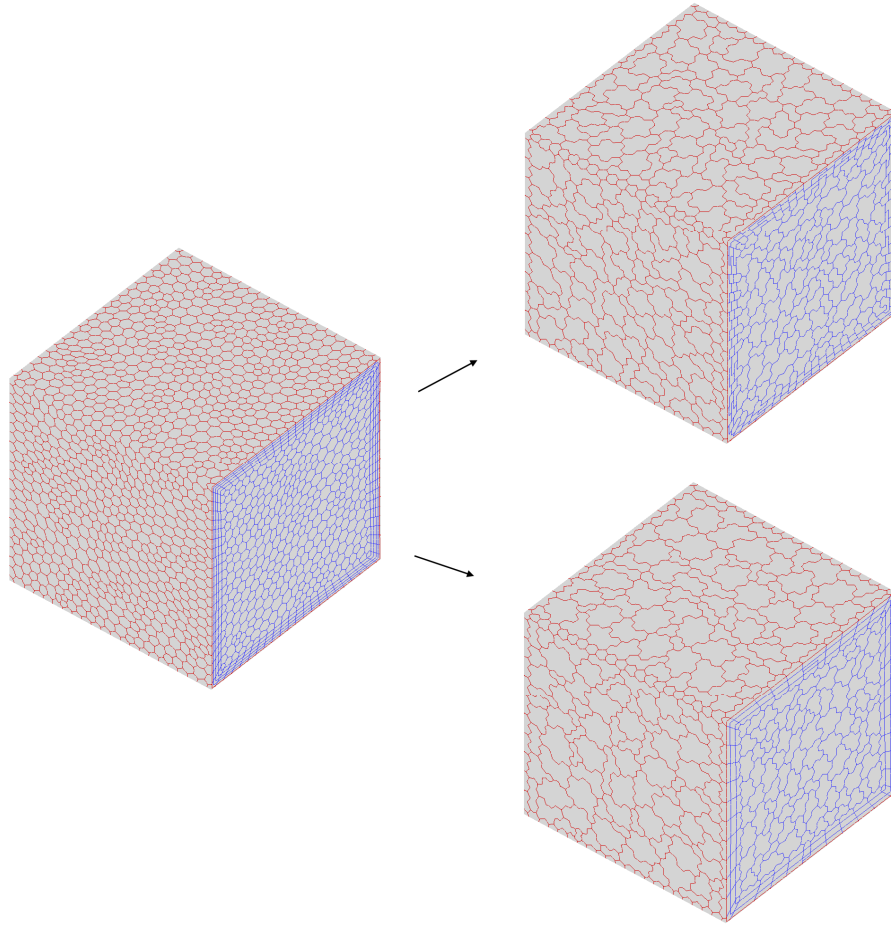


Figure 7: Initial and coarser via isotropic (top) and directional (bottom) fusion surface control-volume grids.

At the first stage of the evaluation, the incorporated full-coarsening directional agglomeration strategy was assessed. Thus, three successively coarser grids were generated, implementing both the isotropic and the directional agglomeration methodology. Figure 7 illustrates the initial and the first-level coarser surface control-volume grids, extracted with both approaches (isotropic-top, directional-bottom). It is obvious that the second agglomeration type preserved more accurately the topology of the initial grid, while it lead to a more extended reduction of DoFs. Contrary to that, the isotropic agglomeration produced arbitrary polyhedral control volumes even in the prismatic region, differentiating significantly the topology of the extracted grid from the initial one. The effect of this differentiation is demonstrated in Figure 8, in-

cluding the radiative intensity convergence history per number of iterations and wall-clock time for two only-spatial S4A1 V(1,0)-cycle simulations, implementing isotropic and directional agglomeration respectively. No significant difference can be identified at the iterations/cycle curve, but the situation is changing at the time curve; particularly, isotropic strategy produced a temporal speed-up coefficient equal to ~ 2.35 for the final residual $1.0E-10$, while directional one equal to ~ 2.51 . Despite a reduction of three or four orders of magnitude is usually more than enough for such test cases, speed-up coefficients have been computed for a final residual value equal to $1.0E-10$, in order the contribution of the proposed multigrid method to be more clearly demonstrated.

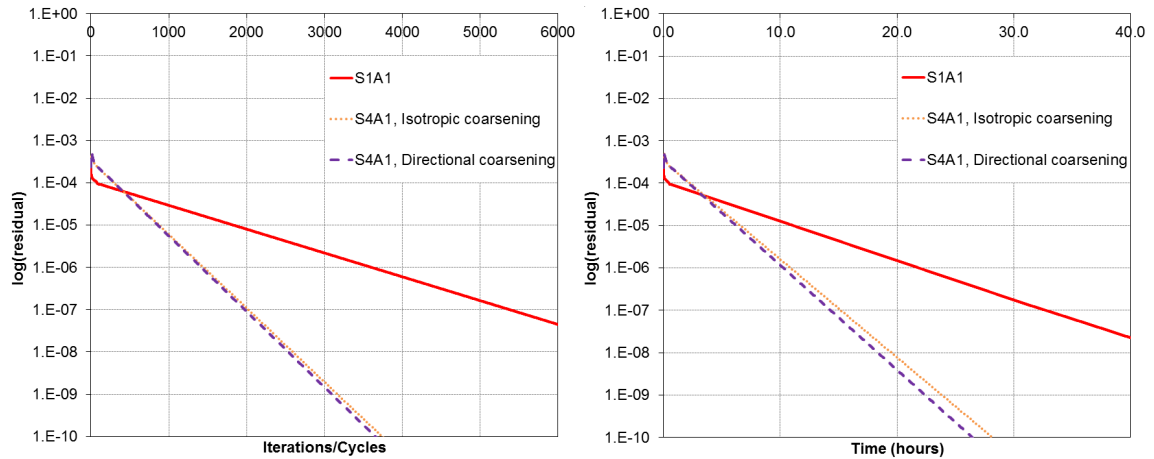


Figure 8: Radiative intensity convergence history per number of iterations and wall-clock time for the only-spatial agglomeration multigrid scheme, implementing isotropic and directional agglomeration approach.

The evaluation of the incorporated multigrid schemes was continued with the only-spatial and only-angular ones implementing though different V-cycle types, namely, V(1,0), V(1,1), V(2,0) and V(2,1). For the implementation of the only-angular as well as of the combined spatial/angular schemes, angular coarsening was performed analogously; the initial finest 16-8 discretization was reduced successively to 8-4 and 4-2. Figures 9 and 10 contain the radiative intensity convergence history per number of iterations and wall-clock time of the aforementioned simulations.

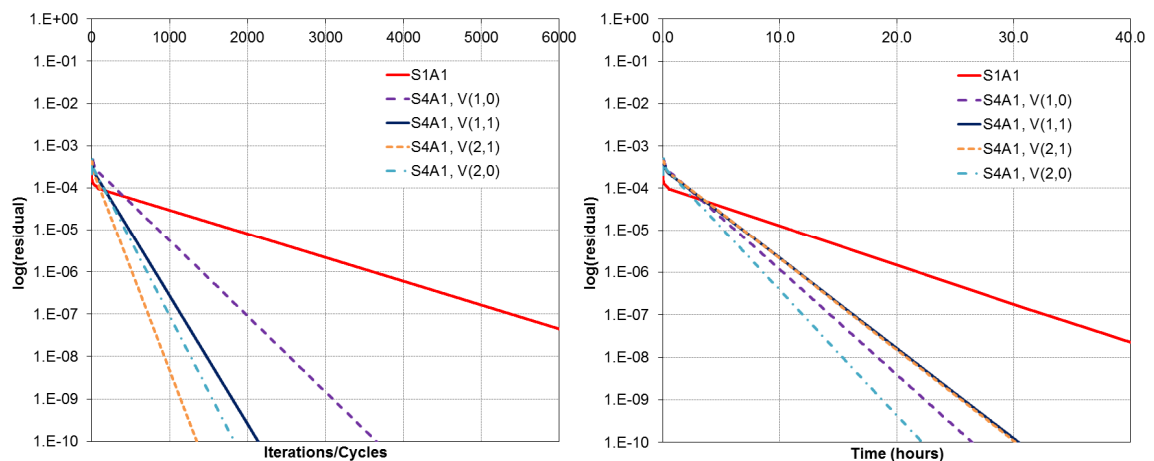


Figure 9: Radiative intensity convergence history per number of iterations and wall-clock time for the only-spatial agglomeration multigrid scheme employing different V-cycle types.

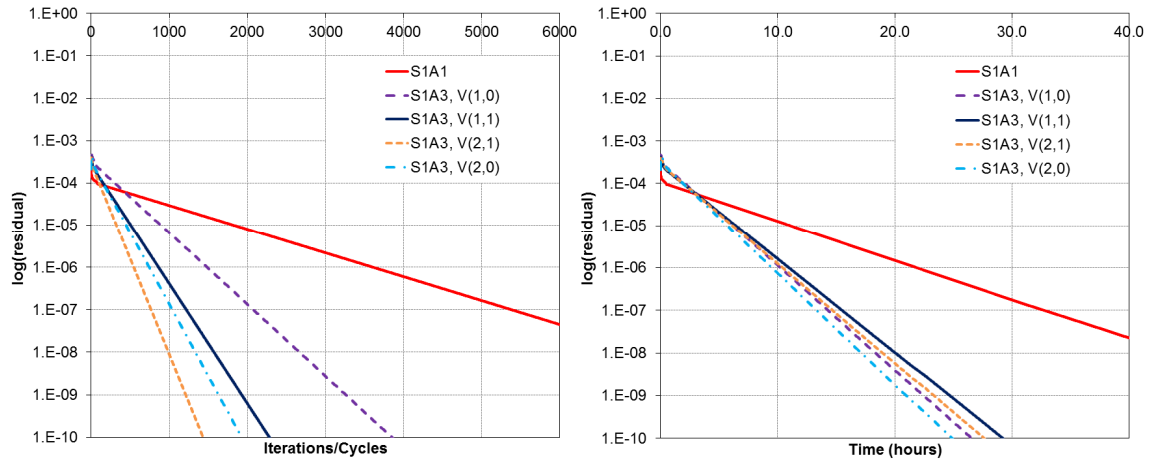


Figure 10: Radiative intensity convergence history per number of iterations and wall-clock time for the only-angular agglomeration multigrid scheme employing different V-cycle types.

The V(2,0)-cycle type seems to be the most efficient one, succeeding a time-acceleration rate equal to ~ 3.00 and ~ 2.67 with the only-spatial and the only-angular multigrid schemes respectively. The V(1,0) is revealed as the next most efficient type, achieving temporal speed-up coefficients equal to ~ 2.51 and ~ 2.49 with the spatial and angular approach respectively. Despite the fact that the only-spatial scheme appears to be more effective than the only-angular one in this test case, the speed-up coefficients (extracted with the V(1,0)-cycle type) of the only-angular scheme highlight the significance of the proposed angular extension to the multigrid technique.

The assessment is continued with simulations implementing the uniform, alternate and nested spatial/angular methodologies, along with the aforementioned V-cycle types. For the fourth FAS level of the uniform and alternate methods (besides the third one), the coarsest angular resolution (4-2) was used as well. Figures 11 to 13 illustrate the radiative intensity convergence history per number of iterations and wall-clock time of the aforementioned simulations. The nested scheme along with the V(2,0)-cycle type appears to derive the most efficient simulation, succeeding a temporal acceleration coefficient equal to ~ 4.21 . The V(2,0)-cycle alternate multigrid approach is revealed as the next most efficient type, with a corresponding coefficient equal to ~ 3.45 . As expected, the aforementioned combined spatial/angular multigrid schemes achieved better temporal rates than the only-spatial or only-angular approaches. Unlike them, the uniform scheme doesn't seem to have a significant effect in the computational performance of the proposed algorithm; actually, it produced worse speed-up coefficients, even compared with the only-spatial or only-angular multigrid methods. This is attributed to the extreme coarsening, entailed by the simultaneous spatial and angular reduction of the corresponding DoFs. Once more the V(2,0)-cycle scheme provided better acceleration coefficients, comparing to the rest V-cycle types, independently of the implemented FAS scheme (uniform, alternate or nested). Furthermore, the simulation involving the nested scheme with the V(1,0)-cycle type failed to converge; this failure originates possibly from the insufficient relaxation of RTE prior prolonging the radiative intensity corrections from the angular to the spatial V-cycle. As far as the rest two V-cycle types are concerned, it seems that the relaxation after the prolongation process does not contribute to the computational performance improvement; on the other hand, it appears to add just extra computation time. The previous state is confirmed from the fact that V(1,1)-cycle type is revealed even slower from the V(2,1).

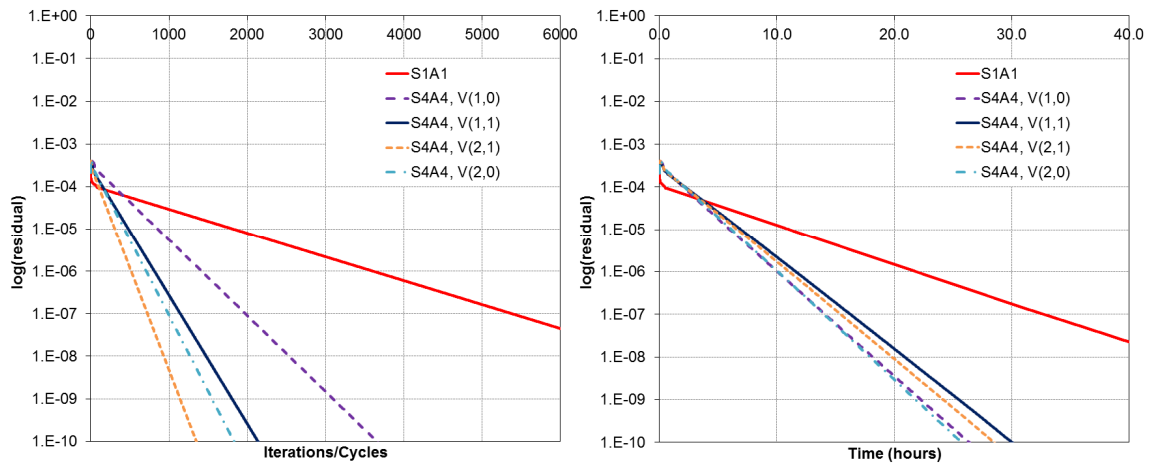


Figure 11: Radiative intensity convergence history per number of iterations and wall-clock time for the uniform spatial/angular agglomeration multigrid scheme employing different V-cycle types.

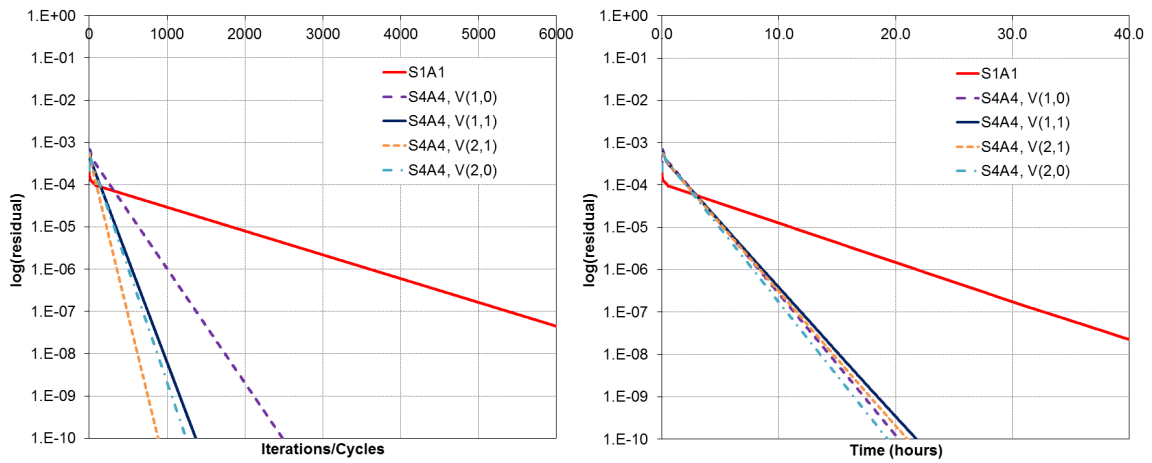


Figure 12: Radiative intensity convergence history per number of iterations and wall-clock time for the alternate spatial/angular agglomeration multigrid scheme employing different V-cycle types.

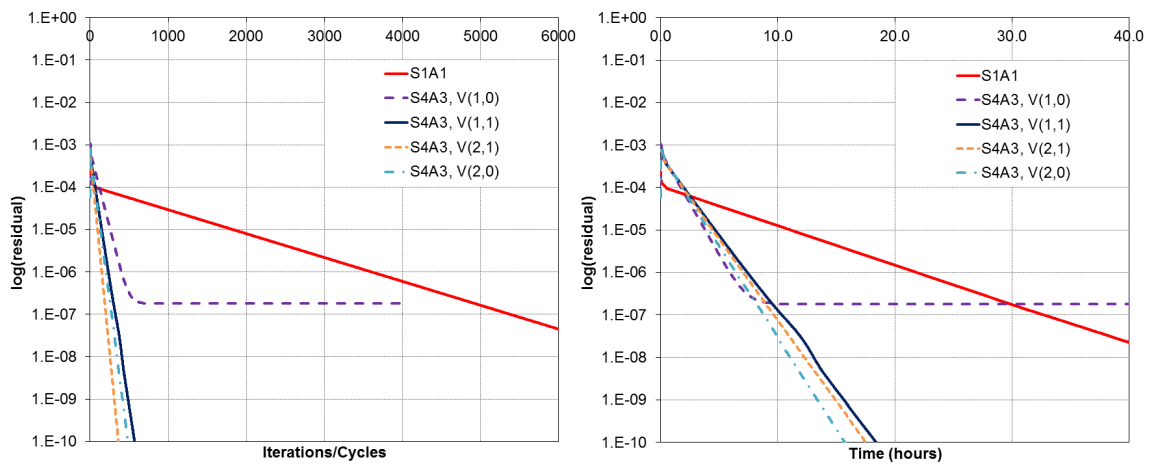


Figure 13: Radiative intensity convergence history per number of iterations and wall-clock time for the nested spatial/angular agglomeration multigrid scheme employing different V-cycle types.

The contribution of the combined FMG-FAS approach was then evaluated for all the incorporated multigrid schemes (only-spatial, only-angular, uniform, alternate and nested). Figure 14 includes the radiative intensity convergence history per number of iterations and wall-clock time of the aforementioned simulations. Different numbers of iterations/cycles were tested for each of the implemented multigrid schemes during the preliminary stage; the most efficient results for each approach are presented in the aforementioned figure. The nested spatial/angular and only-angular methods appear to be the most efficient ones, achieving a temporal speed-up coefficient equal to ~ 4.81 . The next more effective scheme is revealed to be the alternate one, while the only-spatial one provided the worst results; considering the latter observation, the significant contribution of the angular extension of the multigrid technique is once more demonstrated.

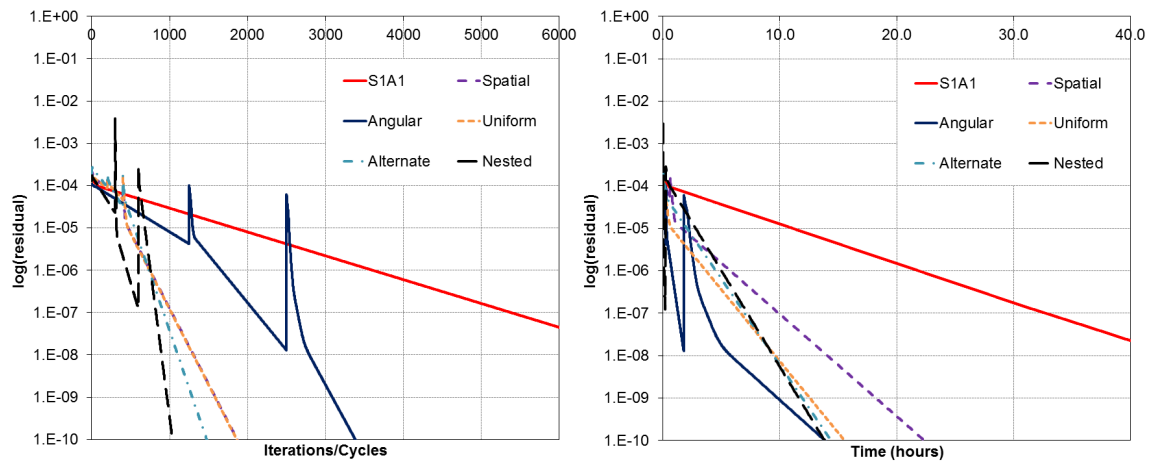


Figure 14: Radiative intensity convergence history per number of iterations and wall-clock time for different combined FMG-FAS agglomeration multigrid schemes.

5 CONCLUSIONS

In this work the development and comparison of different spatial/angular agglomeration multigrid schemes for the acceleration of FVM radiative heat transfer computations, was reported. It was based upon a previous study of the authors [6, 7], incorporating though further enhancements, namely different sequences of spatial and angular coarser resolutions, different V-cycle types, a full-coarsening directional agglomeration strategy and a combined FMG-FAS approach. Based on the results presented in the previous Section, the following conclusions can be extracted: a) Full-coarsening directional agglomeration should be the preferred choice in test cases using hybrid unstructured grids. Unlike the isotropic method, the directional one leads to a deeper reduction of DoFs, while simultaneously it preserves more accurately the topology of the initial grid; as a result a greater efficiency improvement is achieved. b) The V(2,0)-cycle type appears to be superior, compared to the rest tested ones (V(1,0), V(1,1) and V(2,1)), independently of the implemented FAS scheme (only-spatial, only-angular, uniform, alternate or nested). Furthermore, the relaxation after the prolongation process, defined by the latter two types (V(1,1) and V(2,1)), seems not to contribute at all to the computational acceleration. c) The nested spatial/angular agglomeration multigrid approach is revealed to be much more efficient than the rest ones, while the next most effective appears to be the alternate scheme. d) Considering that the aforementioned schemes derived higher acceleration compared to the only-spatial one, as well as the impressive improvement entailed by the only-angular approach, the significant contribution of the angular extension of the mul-

tigrid technique is confirmed. e) Independently of the implemented multigrid scheme (only-spatial, only-angular, uniform, alternate or nested), additional acceleration can be achieved with the implementation of the combined FMG-FAS approach.

REFERENCES

- [1] G.N. Lygidakis, S.S. Sarakinos, I.K. Nikolos, Comparison of different agglomeration multigrid schemes for compressible and incompressible flow simulations, *Advances in Engineering Software*, in press, 2016.
- [2] A. Brandt, Multigrid techniques with applications to fluid dynamics: 1984 guide, *VKI Lecture Series*, 1-176, 1984.
- [3] J. Blazek, *Computational Fluid Dynamics: Principles and Applications*, Kidlington, Elsevier Science, 2001.
- [4] G.N. Lygidakis, I.K. Nikolos, Numerical analysis of flow over the NASA common research model (CRM) using the academic CFD code Galatea, *ASME Journal of Fluids Engineering*, vol. **137**, 071103, 2015.
- [5] H. Nishikawa, B. Diskin, Development and application of parallel agglomerated multigrid methods for complex geometries, *20th AIAA Computational Fluid Dynamics Conference*, Honolulu, Hawaii, USA, June 27-30, 2011, AIAA 2011-3232.
- [6] G.N. Lygidakis, I.K. Nikolos, Using a parallel spatial/angular agglomeration multigrid scheme to accelerate the FVM radiative heat transfer computation – part I: Methodology, *Numerical Heat Transfer, Part B: Fundamentals*, **66**, 471-497, 2014.
- [7] G.N. Lygidakis, I.K. Nikolos, Using a parallel spatial/angular agglomeration multigrid scheme to accelerate the FVM radiative heat transfer computation – part II: Numerical results, *Numerical Heat Transfer, Part B: Fundamentals*, **66**, 498-525, 2014.
- [8] G. Kim, S. Kim, Y. Kim, Parallelized unstructured-grid finite volume method for modeling radiative heat transfer, *Journal of Mechanical Science and Technology*, **19**, 1006-1017, 2005.
- [9] R. Capdevila, C.D. Perez-Segarra, A. Oliva, Development and comparison of different spatial numerical schemes for the radiative transfer equation resolution using three-dimensional unstructured meshes, *Journal of Quantitative Spectroscopy and Radiative Transfer*, **111**, 264-273, 2010.
- [10] G.N. Lygidakis, I.K. Nikolos, Using a high-order spatial/temporal scheme and grid adaptation with a finite-volume method for radiative heat transfer, *Numerical Heat Transfer, Part B: Fundamentals*, **64**, 89-117, 2013.
- [11] G.N. Lygidakis, I.K. Nikolos, Improving the accuracy of a finite-volume method for computing radiative heat transfer in three-dimensional unstructured meshes, *3rd South-East European Conference on Computational Mechanics, ECCOMAS-IACM Special Interest Conference*, Kos, Greece, June 12-14, 2013, 599-620.
- [12] P. Hassanzadeh, G.D. Raithby, Finite-volume solution of the second order radiative transfer equation: Accuracy and solution cost, *Numerical Heat Transfer, Part B: Fundamentals*, **53**, 374-382, 2008.

-
- [13] M.H. Lallemand, *Schemas decentres multigrilles pour la resolution des equations d' Euler en elements finis*, PhD Thesis, Universite de Provence, France, 1988.
- [14] D.J. Mavriplis, Directional coarsening and smoothing for anisotropic Navier-Stokes problems, *Electronic Transactions in Numerical Analysis*, **6**, 182-197, 1997.
- [15] N.K. Lambropoulos, D.G. Koubogiannis, K.C. Giannakoglou, Acceleration of a Navier-Stokes equation solver for unstructured grids using agglomeration multigrid and parallel processing, *Computer Methods in Applied Mechanics and Engineering*, **193**, 781-803, 2004.
- [16] H. Nishikawa, B. Diskin, J.L. Thomas, Recent advances in agglomerated multigrid, *15th AIAA Aerospace Sciences Meeting*, Grapevine, Texas, USA, January 7-10, 2013, AIAA 2013-0863.
- [17] V. Hannemann, Structured multigrid agglomeration on a data structure for unstructured meshes, *International Journal for Numerical Methods in Fluids*, **40**, 361-368, 2002.
- [18] G.N. Lygidakis, I.K. Nikolos, Using the finite-volume method and hybrid unstructured meshes to compute radiative heat transfer in 3-D geometries, *Numerical Heat Transfer, Part B: Fundamentals*, **62**, 289-314, 2012.
- [19] T.K. Kim, H. Lee, Effect of anisotropic scattering on radiative heat transfer in two-dimensional rectangular enclosures, *International Journal of Heat and Mass Transfer*, **31**, 1711-1721, 1988.
- [20] B. Hunter, Z. Guo, Comparison of the discrete-ordinates method and the finite-volume method for steady-state and ultrafast radiative transfer analysis in cylindrical coordinates, *Numerical Heat Transfer, Part B: Fundamentals*, **59**, 339-359, 2011.
- [21] G.D. Raithby, Discussion of the finite volume method for radiation, and its application using 3D unstructured meshes, *Numerical Heat Transfer, Part B: Fundamentals*, **35**, 389-405, 1999.
- [22] H. Jimbo, R. Liming, T. Heping, Effect of anisotropic scattering on radiative heat transfer in two-dimensional rectangular media, *Journal of Quantitative Spectroscopy and Radiative Transfer*, **78**, 151-161, 2003.
- [23] G.D. Van Albada, B. Van Leer, W.W. Roberts, A comparative study of computational methods in cosmic gas dynamics, *Journal of Astrophysics and Astronomy*, **108**, 46-84, 1982.
- [24] P.K. Sweby, High resolution schemes using flux limiters for hyperbolic conservation laws, *SIAM Journal for Numerical Analysis*, **21**, 995-1011, 1984.
- [25] M.H. Lallemand, *Etude de schemas Runge-Kutta a 4 pas pour la resolution multigrille des equations d' Euler 2D*, Raport de Recherche, INRIA, 1988.
- [26] V. Venkatakrishnan, Implicit schemes and parallel computing in unstructured grid CFD, *26th Computational Fluid Dynamics Lecture Series Program, VKI*, Rhode Saint-Genese, Belgium, March 13-17, 1995.
- [27] S. Lanteri, Parallel solutions of compressible flows using overlapping and nonoverlapping mesh partitioning strategies, *Parallel Computing*, **22**, 943-968, 1996.